NUMERICAL STUDY OF SiO_2-Al_2O_3/$C_2H_6O_2$ HYBRID NANOFLUID FLOW PAST A WEDGE IN THE PRESENCE OF DISSIPATIVE AND RADIATIVE EFFECTS

[1]Sonika Sharma, [2]Shilpa Sood

[1]*Department of Mathematics and Statistics, Career Point University, Hamirpur (H.P.).*

[2]*Department of Mathematics and Statistics, Career Point University, Hamirpur (H.P.).*

Corresponding Author: Sonika Sharma

Affiliation: Research Scholar

Abstract

Viscous and radiation impacts with Darcy-Forchheimer flow on two-dimensional boundary layer flow across the stretching wedge are looked at in this study. Here, ethylene glycolis addressed as a conventional fluid with dispersion of silicon oxide and aluminum oxide nanoparticles. We've developed a mathematical framework for simulating hybrid nanofluids' physical properties. Employing similarity mechanisms, the highly nonlinear paired partial differential equations are turned into dimensionless ordinary differential equations. Then, the MATLAB based bvp4C solver is utilized to find the solution. Figures and tables explain the impact of flow-controlling parameters. In the next sections, tables of interesting physical parameters (such as friction factors and Nusselt numbers) are presented for a range of prominent parameters.

Keywords *Hybrid nanofluid, Stretching wedge, Darcy Forchheimer flow, Viscous dissipation, Boundary layer flow, Thermal radiation.*

1   Introduction

The border line flow across a wedge-shaped object with heat transfer has emerged as a popular topic in fluid mechanics over the last few decades. Thermal insulation heat exchangers, polymer processing, crude oil drilling, liquid metal flow in heat exchangers, air cooling in air conditioners, geothermal systems, nuclear power plants, the design of straps on aero plane wings for strengthen lift, drag and maneuverability, warship and submarine modelling, the storage of nuclear waste, etc. are some of the applications of flow past a wedge. The wedge flow concept was firstly introduced by Falkner and Skan [1]. Prandtl boundary layer idea was used by Falkner–Skan to develop the wedge flow model. An equation for the boundary layer can be transformed to a simple differential equation (the Falkner-Skan equation) by applying similarity techniques. Flows that are not uniform, such as outer flows that are estimated at the wall as ax^m, where $a > 0$ and m are constants, are included in this equation. Numerous studies have been done about the implementations to Falkner-Skan equation, including Hartree [2], Stewartson [3], Chen and Libby [4], Rajagopal et al. [5], Botta et al. [6], Brodie and Banks [7], Heeq et al. [8], Zaturska and Banks [9], Kumari et al. [10], Kuo [11], Pantokratoras[12], Ishak et al. [13] and so forth. Hydromagnetic convection was examined by Vajravelu and Nayfeh [14] in a wedge and a cone. A non-isothermal wedge in the existence of the radiative heat effect is studied by Chamkha et al. [15]. Ahmad and Khan [16] explored a moving wedge with convection to determine the viscous dissipative influence on heat generation and absorption. Utilizing the spectral quasilinearization method, Ibrahim and Tulu [17] have analyzed numerically the problem of boundary layer flow across a wedge immersed in porous media saturated with nanofluid with MHD and viscous dissipation impact. It was recently

reported that the stretching wedge of Casson fluid had been examined empirically by Bano et al. [18].

For researchers and scientists, the flow of normal fluids or nanofluids through a wedge surface opens up a new avenue of opportunity. As a result, researchers and scientists concentrated their efforts in this direction and improved considerably the model with each passing day. conventional liquids (ethylene glycol, oil, and water) cannot fulfil today's expectations due to their restricted heat transmission capabilities. As a result, the most recent generation of highthermal expansion fluids, known as nanofluids, are being successfully deployed in the industrial sector. As a solid-liquid mixture, a nanofluid consists of a traditional fluid and nano-sized particles. Nanofluids have excellent thermophysical properties due to their tiny size and high surface area unique to the nanoparticles; as a result, they may be used widely in MEMS and nanotechnology applications.

Many researchers have been intrigued by a new hybrid nanofluid because of its exceptional thermal conductivity after extensive research into nanofluid in general. Hybrid nanofluids are a magnificent functioning liquid that combines two different types of nanoparticles with diameter (under 100 nm) into the regular fluids (water, blood, oils etc.). Heat transfer coefficients and the thermal conductivity of these liquids are much higher than those of ordinary liquids. These hybrid nanofluids have recently been employed in a variety of heat transfer applications, such as coolant in machining and manufacturing, acoustics, micro fluidics as well as biomedical, space and naval constructions. They have also been used in solar energy, refrigeration and heating. Hybrid nanofluid, which is an expansion of nanofluid, is known to be good at transferring heat. To achieve the homogeneous phase properties, the hybrid nanomaterial combines the chemical and physical characteristics of many nanomaterials simultaneously. Heat transfer and pressure drop specifications change a lot when hybrid nanofluids are used instead of standard nanofluids. It's because hybrid nanofluids have a higher aspect ratio, a more effective thermal network, and a larger number of nanoparticles working together. Despite this, the long-term stability of nanofluids, the manufacturing process, the right nanoparticles composition to achieve synergistic effects, and the high cost of nanofluids might be the main barriers and even not be feasible for real-world use [19]. Sarkar et al., Sunder et al., Sidik et al., and Sajid et al. have documented in detail the previous and present research and development corelated to hybrid nanofluid preparation techniques, thermophysical characteristics of hybrid nanofluids, and recent applications of hybrid nanofluids. [20]-[23]. Devi and Devi [24] investigated the flow of a hybrid nonfluid over a stretching sheet utilizing

$Cu - Al_2O_3$ nanoparticles with magnetic effects. It was then expanded to three-dimensional flow under Newtonian heating conditions in the work of Devi and Devi [25]. Hybrid nanofluid was found to have a higher heat transfer rate than conventional nanofluid in both studies. The impact of water-based hybrid nano liquid through mixing nanoparticles (TiO_2, SiO_2 and Al_2O_3) with varying viscosity was calculated by Adriana et al. [26]. Rostami et al. [27] examined the effect of magnetic field on free and forced convection flow of hybrid SiO_2–Al_2O_3–H_2O nanofluids from a porous vertical surface. Few recent published studies on hybrid nanofluids are described in references [28]-[32].

Inspired by the studies described above, in the present paper, we explored Darcy-Forchheimer flow due to SiO_2-Al_2O_3/$C_2H_6O_2$ hybrid nanofluid in the presence of dissipative and radiative flow past a wedge by deploying the Tiwari and Das nanofluid model [33]. The solid volume fractions of the nanoparticles are taken into account in this model. The results for velocity distribution, temperature distribution, skin friction coefficient and Nusselt number are portrayed through graphs and tables and debated briefly.

2   Flow Modelling of the Problem

Physical description

Consider an incompressible steady two-dimensional boundary layer flow with viscous and radiation effects over a wedge embedded in Darcy Forchheimer flow as depicted in Fig. 1. We have employed Al_2O_3 and SiO_2 as nanoparticles in conjunction with ethylene glycol as regular fluid. Suppose that the wedge moves with velocity $U_w(x)$, $U_\infty(x)$ is free-flow velocity , whereas T_w is temperature at wall and T_∞ is ambient temperature. The temperature change inside the flow is expected to be minimal. The x-axis is regarded as being parallel to the wedge's surface, whereas the y-axis is regarded as being perpendicular. Similarily, $\beta = \dfrac{2m}{1+m}$ and $\Omega = \beta\pi$, where β, m and Ω are Hartee pressure gradient, moving Wedge angle parameter and wedge angle respectively.
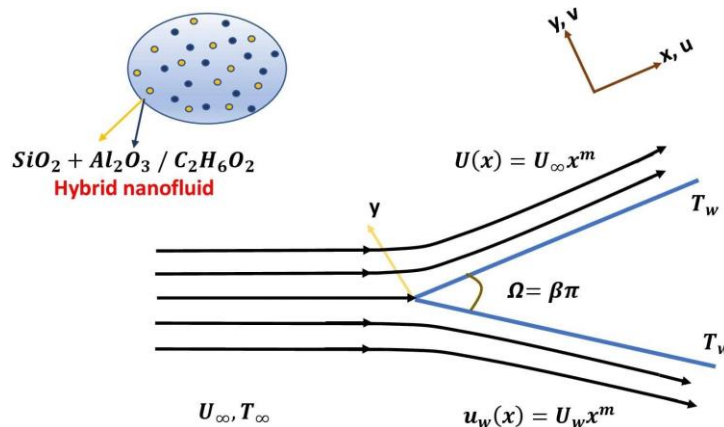
Figure 1: Diagrammatic representation of the problem

Leading equations

The steady leading equations for hybrid nanofluids are given as below:

$$\frac{\partial u}{\partial x} + \frac{\partial v}{\partial y} = 0, \tag{1}$$

$$u\frac{\partial u}{\partial x} + v\frac{\partial u}{\partial y} = U\frac{dU}{dx} + \frac{\mu_{hnf}}{\rho_{hnf}}\frac{\partial^2 u}{\partial y^2} - \frac{v_{hnf}}{K}u - \frac{F}{\rho_{hnf}}u^2, \tag{2}$$

$$u\frac{\partial T}{\partial x} + v\frac{\partial T}{\partial y} = \alpha_{hnf}\frac{\partial^2 T}{\partial y^2} - \frac{1}{(\rho c_p)_{hnf}}\frac{\partial q_r}{\partial y} + \frac{\mu_{hnf}}{(\rho c_p)_{hnf}}\left(\frac{\partial u}{\partial y}\right)^2, \tag{3}$$

where u and v signify velocities towards the x and y axes. Here, K specifies permeability of the porous medium, F represents the non-uniform inertia coefficient of porous medium, μ_{hnf}, ρ_{hnf}, α_{hnf} and $(\rho c_p)_{hnf}$ describe the dynamic viscosity, the effective dynamic density, the thermal diffusivity and heat capacitance respectively.

The Rosseland approximation is used to evaluate and simplify the radioactive heating flux in the temperature equation, i.e.,

$$q_r = \frac{4\sigma^*}{3K^*}\frac{\partial T^4}{\partial y} \tag{4}$$

where K^* describes the Stefan-Boltzmann constant and σ^* is the mean absorption coefficient. Consequently, T^4 can be regarded as a linear function of temperature ignoring the higher orderterms, whereas T^4 can be generalized in Taylor series about T_∞ which is derived as follow [37]:

$$T^4 = T_\infty^4 + 4T_\infty^3(T - T_\infty)^2 + 6T_\infty^2(T - T_\infty)^2 + ... \tag{5}$$

We get the following result if we ignore the higher-order terms of the previously stated assertion beyond the first degree in the series:

$$T^4 \cong 4TT_\infty^3 - 3T_\infty^3 \tag{6}$$

Thus

$$\frac{\partial q_r}{\partial y} = -\frac{16T_\infty^3\sigma^*}{3K^*}\frac{\partial^2 T}{\partial y^2} \tag{7}$$

Using Eq.(8), the energy Eq. (3) be reduced to

$$u\frac{\partial T}{\partial x} + \frac{\partial T}{\partial y} = \alpha_{hnf}\frac{\partial^2 T}{\partial y^2} + \frac{1}{(\rho c_p)_{hnf}}\frac{16T_\infty^3\sigma^*}{3K^*}\frac{\partial^2 T}{\partial y^2} + \frac{\mu_{hnf}}{(\rho c_p)_{hnf}}\left(\frac{\partial u}{\partial y}\right)^2 \tag{8}$$

Boundary conditions

Subject to the boundary conditions

$$\{u = U_w(x),\ v = 0,\ T = T_w\}\ at\ y = 0,$$
$$u = U_\infty(x),\ T \rightarrow T_\infty,\ as\ y \rightarrow \infty \tag{9}$$

Non-dimensionalization

The similarity transformations are introduced

$$\psi = \sqrt{\frac{2x v_f U(x)}{(m+1)}}\ f(\eta),$$

$$\eta = \sqrt{\frac{(m+1)U(x)}{2x v_f}}\ y, \tag{10}$$

$$\theta(\eta) = \frac{T - T_\infty}{T_f - T_\infty}$$

$$u = \frac{\partial \psi}{\partial y} = a x^m f'(\eta); \quad v = -\frac{\partial \psi}{\partial x} = -\frac{(m-1)a x^{(m-1)}}{2} y f'(\eta) - \sqrt{\frac{(m+1)v_f a x^{m-1}}{2}}\ f(\eta).$$

By substituting the similarity variables (10) into Eqs. (1),(2) and (8), we get as follows:

$$f''' + \frac{\rho_{hnf}/\rho_f}{\mu_{hnf}/\mu_f}\left[\beta(1 - f'^2) + ff'\right] - Lf' - \frac{\mu_f}{\mu_{hnf}}F_r f'^2 = 0 \tag{11}$$

$$\left(\frac{k_{hnf}}{k_f} - \frac{4}{3}R\right)\theta'' + \frac{\mu_{hnf}}{\mu_f}Pr\ Ec\ f''^2 + (\rho c_p)_{hnf}/(\rho c_p)_f\ Pr\ f\ \theta' = 0 \tag{12}$$

restricted to boundary conditions

$$f(0) = 0,\ f'(0) = \lambda,\ \theta(0) = 1, \tag{13}$$

$$f'(\infty) \rightarrow 1,\ \theta(\infty) \rightarrow 0. \tag{14}$$

Here, Hartee pressure gradient (β), wedge angle parameter (m), porosity parameter (L), Forchheimer number (Fr), radiation parameter(R), Prandtl number (Pr), Eckert number (Ec), and the constant moving wedge parameter (λ) are figure out as follow:

$$\beta = \frac{2m}{m+1},\ m = \frac{\beta}{(\beta-2)},\ L = \frac{2v_f x^{1-m}}{Ka(m+1)},\ Fr = \frac{2Fx}{(m=1)},\ R = \frac{4\sigma^* T_\infty^3}{K^* k_f},$$

$$Pr = \frac{\mu_f(c_p)_f}{k_f},\ Ec = \frac{U^2(x)}{(c_p)_f(T_w - T_\infty)},\ \lambda = \frac{U_w}{U_\infty}.$$

2.5 Physical quantities of engineering interest

When it comes to heat flow, the two most important physical quantities are the local rate of heat transfer (the Nusselt number) and the skin friction factor. The coefficient of skin friction C_f and the local Nusselt number Nu_x are structured as below:

$$C_f = \frac{\tau_w}{\rho_f U^2(x)}, \quad Nu_x = \frac{x q_w}{k_f(T_w - T_\infty)} \tag{15}$$

where, shear stress and heat flux from the surface of the wedge are depicted by τ_w and q_w, respectively, which are illustrated by

$$\tau_w = \mu_{hnf}\left(\frac{\partial u}{\partial y}\right)_{y=0}, \quad q_w = -k_{hnf}\left(\frac{\partial T}{\partial y}\right)_{y=0} + (q_r)_{y=0} \tag{16}$$

Using Eq.(10), (15) and (16), we get

$$(Re_x)^{1/2} C_f = \frac{1}{(1-\phi_1)^{2.5}(1-\phi_2)^{2.5}} f''(0)\left(\frac{m+1}{2}\right)^{1/2},$$
$$(Re_x)^{-1/2} Nu_x = -\left(\frac{k_{nf}}{k_f} + \frac{4}{3}R\right)\theta'(0)\left(\frac{m+1}{2}\right)^{1/2}, \tag{17}$$

where $Re_x = \dfrac{a x^{m+1}}{\nu_f}$ signifies the local Reynolds number.

Method of Solution

In this segment, MATLAB's boundary value problem solver bvp4c is used to figure out the non-linear ordinary differential equations (11) and (12) that govern the leading partial differential equations (2) and (3). The non-dimensional variables in these equations are used to simplify them. The purpose of simplifying ordinary differential equations is to make them easier to solve numerically. This section will go into detail about how the bvp4c is implemented for the current problem. In steps 1 and 2, we explored how to convert the system of ordinary differential equations for the current situation to a system of five first order equations. The boundary condition is converted in step 3 and the remaining of the program is accomplished in step 4.

Step 1:

First and foremost, we'll introduce some components for the paired non-linear Ordinary differential equations in Eqs.(11), (12) and (13):

$$f = y(1), f' = y(2), f'' = y(3)$$
$$\theta = y(4), \theta' = y(5),$$

(18)

Step 2:

Now, in the first order system of equations, we will write these new components as follows:

$$f' = y(2), f'' = y(3),$$

$$f''' = -\frac{\rho_{hnf}/\rho_f}{\mu_{hnf}/\mu_f} \left[\beta(1 - y(2)^2) + y(1)\, y(3)\right] + L\, y(1) + \frac{\mu_f}{\mu_{hnf}} Fr\, y(2)^2$$

$$\theta = y(4), \theta' = y(5),$$

(19)

$$\theta'' = -\frac{1}{\left((k_{hnf}/k_f) - \frac{4}{3}R\right)} \left[\frac{\mu_{hnf}}{\mu_f} Ec\, Pr\, y(3)^2 + \frac{(\rho c_p)_{hnf}}{(\rho c_p)_f} Pr\, y(1)\, y(5)\right]$$

Step 3:

In accordance with the new components, the boundary conditions are translated into:

$$ya(1) = 0,\ ya(2) = -\lambda,\ ya(4) = 1,\ yb(2) = 1,\ yb(4) = 0$$

(20)

Step 4:

MATLAB's bvp4c solver is used to solve the system of first-order equations with boundary conditions.

Result and Discussion

Table 1: Thermophysical characteristics of regular fluid and considering nanoparticles [38]-[39]

Base fluid and nanoparticles	$\rho(kg/m^3)$	$c_p(J/kgK)$	$\kappa(W/mK)$
Ethylene glycol ($C_2H_6O_2$)	1113.5	2430	0.253
Silica (SiO_2)	2650	730	1.5
Alumina (Al_2O_3)	3970	765	40

The findings of velocity profile $f(\eta)$ and temperature profile $\theta(\eta)$ for Hartee pressure gradient (β), wedge angle parameter (m), porosity parameter(L), Forchheimer number (Fr), radiation component (R), Prandtl number (Pr), Eckert number (Ec), and constant moving wedge component (λ) are explored in this segment. Tables 3 and 4 show that the validity of current study can be verified by comparing its findings to those of previous studies. The impact of regulating variables on the fluctuation of skin friction and Nusselt number is demonstrated in Tables 4 and 5. It is noticed that the skin friction coefficient escalates with escalating values of φ_1, φ_2, and m. Table 4 depicts that Nusselt number shows increasing behavior for increasing values of φ_1, φ_2, Pr, Ec, λ and R while decreases for m, L and Fr.

Fig. 2a determines the impact of the wedge angle factor on the nanofluid velocity. Fig. 2a and Fig. 2b reveals that the nanofluid velocity declines and thermal boundary layer thickness grows as the wedge parameter is raised. The influence of the Forchheimer number Fr over dimensionless velocity and temperature is depicted in Fig. 3a and Fig. 3b. Figures assure that as Fr is elevated, the stream-wise velocity component $f'(\eta)$ rises and the fluid temperature decreases in the boundary layer region.

Table 2: Applied models for thermophysical characteristics of nanofluid and hybrid nanofluid [34]-[36].

Property	Nanofluid	Hybrid nanofluid
Density	$\rho_{nf}=(1-\phi_1)\rho_f+\phi_1\rho_{s1}$	$\rho_{hnf}=(1-\phi_2)((1-\phi_1)\rho_f+\phi_1\rho_{s1})+\phi_2\rho_{s2}$
Heat capacity	$(\rho c_p)_{nf}=(1-\phi_1)(\rho c_p)+\phi_1(\rho c_p)_{s1}$	$(\rho c_p)_{hnf}=(1-\phi_2)((1-\phi_1)(\rho c_p)_f+\phi_1(\rho c_p)_{s1})+\phi_2(\rho c_p)_{s2}$
Dynamic viscosity	$\mu_{nf}=\dfrac{\mu_f}{(1-\phi_1)^{2.5}}$	$\mu_{hnf}=\dfrac{\mu_f}{(1-\phi_1)^{2.5}(1-\phi_2)^{2.5}}$
Thermal conductivity	$\dfrac{\kappa_{nf}}{\kappa_f}=\dfrac{\kappa_{s1}+2\kappa_f-2\phi_1(\kappa_f-\kappa_{s1})}{\kappa_{s1}+2\kappa_f+\phi_1(\kappa_f-\kappa_{s1})}$	$\dfrac{\kappa_{hnf}}{\kappa_{nf}}=\dfrac{\kappa_{s2}+2\kappa_{nf}-2\phi_2(\kappa_{nf}-\kappa_{s2})}{\kappa_{s2}+2\kappa_{nf}+\phi_2(\kappa_{nf}-\kappa_{s2})}$ where $\dfrac{\kappa_{nf}}{\kappa_f}=\dfrac{\kappa_{s1}+2\kappa_f-2\phi_1(\kappa_f-\kappa_{s1})}{\kappa_{s1}+2\kappa_f+\phi_1(\kappa_f-\kappa_{s1})}$

Fig. 4a displays the impact of the porosity variable L on the velocity distribution. The fluidflow is restricted by the permeability of the surface when the porosity parameter is increased. It can be noticed that when the value of L grows, the velocity in the boundary layer region accelerates. As a result, by growing value of L, the momentum boundary layer thickness is reduced. When the medium has a high porosity, i.e., when L is increased, the fluid has more area to flow and, as a result, its velocity increases. The Darcian body force reduces flow behavior in the boundary layer because it is inversely proportional to the porosity of the medium. Furthermore, as illustrated in Fig 4b, the temperature distribution declines as the porosity parameter L is increased. As the porosity parameter L is raised, the thermal boundarylayer thins out.

Table 3: Comparative analysis for $f'(0)$ when $M = \beta = Fr = \varphi = 0$ for numerous values of m.

m	White [40]	Khan and Pop [41]	Present Study
0	0.4696	0.4696	0.4696
1/11	0.6550	0.6550	0.6550
1/5	0.8021	0.8021	0.8021
1/3	0.9277	0.9277	0.9277
1/2	1.0389	1.0389	1.038
1	1.2326	1.0389	1.0389

Fig. 5a and Fig. 5b illustrate the influence of λ on $f'(\eta)$ and $\theta(\eta)$. Fig. 6 and Fig. 7 portrayed the effects of nanoparticle volume fractions φ_1 and φ_2 on the velocity and temperature distributions of the fluid. The fluid velocity diminishes and the temperature profile improves when hybrid nanoparicles are strengthened. Fig. 8a demonstrated the influence of radiation variable on temperature distribution. It is noteworthy to see that when the radiation component goes up, the temperature goes down. The Eckert number characterizes heat transfer dissipation by relating flow kinetic energy to boundary layer enthalpy difference. Fig. 8b illustrates the Eckert number influence on the hybrid nanofluid temperature field. Fig. 8c displays how the Prandtl number affects the temperature of nanofluids. The Prandtl number governs the relative thermal boundary layer thickness in heat exchange analysis. Heat dissipates more slowly when the Prandtl number is high. This implies that as Prandtl number grows, the thermal boundary layer thickness diminishes. As a result, as the Prandtl number rises, heat diffusion diminishes, hence impeding the melting process.

Table 4: Comparative analysis for the temperature gradient $-\theta'(0)$ when $M = \beta = Fr = \varphi = 0$.

m	Blasius [42]	Khan and Pop [41]	Present Study
0	0.8769	0.8769	0.8769
1	1.279	1.279	1.1279

Table 5: Computation of the skin friction coefficient for varying values of φ_1, φ_2, and m with $Pr = 1$, $R = 2$, and $L = Ec = Fr = \lambda = 0$.

ϕ_1	ϕ_2	m	$\dfrac{1}{(1-\phi_1)^{2.5}(1-\phi_2)^{2.5}}f''(0)\left(\dfrac{m+1}{2}\right)^{1/2}$
0.01	0.01	0.4	0.85433
0.02			0.87575
0.03			0.89756
0.04			0.91980
	0.02		0.87086
	0.03		0.88775
	0.04		0.90502
		0.1	0.51908
		0.2	0.64949
		0.3	0.75864

Table 6: Computation of local Nusselt number for various values of φ_1, φ_2, m, Pr, L, Ec, Fr, λ and R.

ϕ_1	ϕ_2	m	Pr	L	Ec	Fr	λ	R	$-\left(\dfrac{k_{nf}}{k_f}+\dfrac{4}{3}R\right)\theta'(0)\left(\dfrac{m+1}{2}\right)^{1/2}$
0.01	0.01	0.4	1	-2	2	0.1	1	-2	-0.02902
0.02									-0.02902
0.03									-0.01198
0.04									-0.00340
	0.02								-0.01697
	0.03								-0.00484
	0.04								0.00737
		0.1							0.16141
		0.2							0.08355
		0.3							0.02151
			2						0.13948
			3						0.31961
			4						0.50634
				-1					-0.30278
				0					-0.56936
				1					1.03766
					0				-0.38741
					1				-0.20821
					3				0.15017
						0.2			-0.03892
						0.3			-0.04914
						0.4			-0.05970
							2		1.64800
							3		5.19607
							4		10.943
								-3	-0.13055
								-2	-0.02902
								-1	0.011189

Figure 2: Variation of m on $f'(\eta)$ and $\theta(\eta)$.
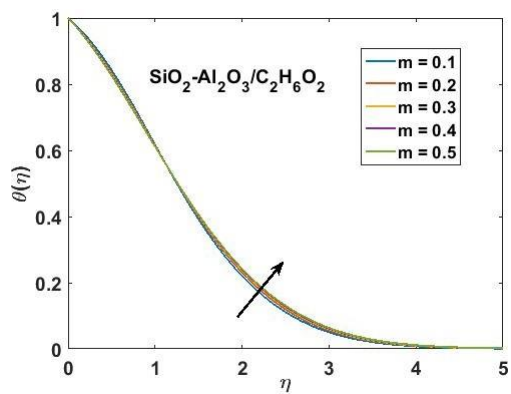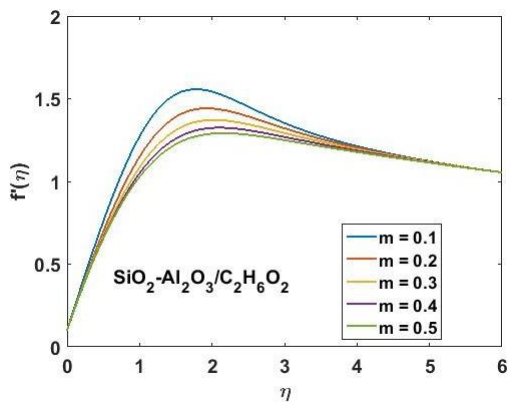
(a) Velocity profile $f'(\eta)$ for diverging amounts of m (b) Thermal profile $\theta(\eta)$ for deviating values of m

Figure 3: Variation of Fr on $f'(\eta)$ and $\theta(\eta)$.
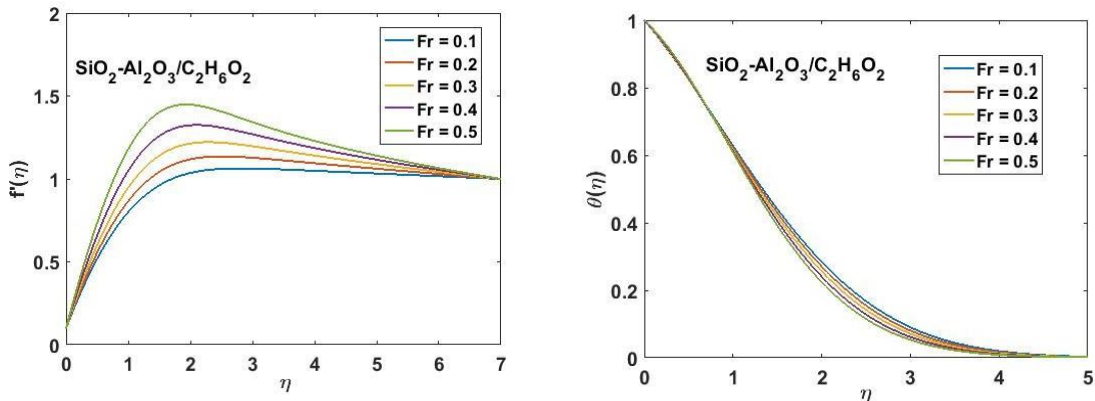
(a) Velocity profile $f'(\eta)$ for diverging amounts of Fr

(b) Thermal profile $\theta(\eta)$ for diverging amounts of Fr

Figure 4: Variation of L on $f'(\eta)$ and $\theta(\eta)$.
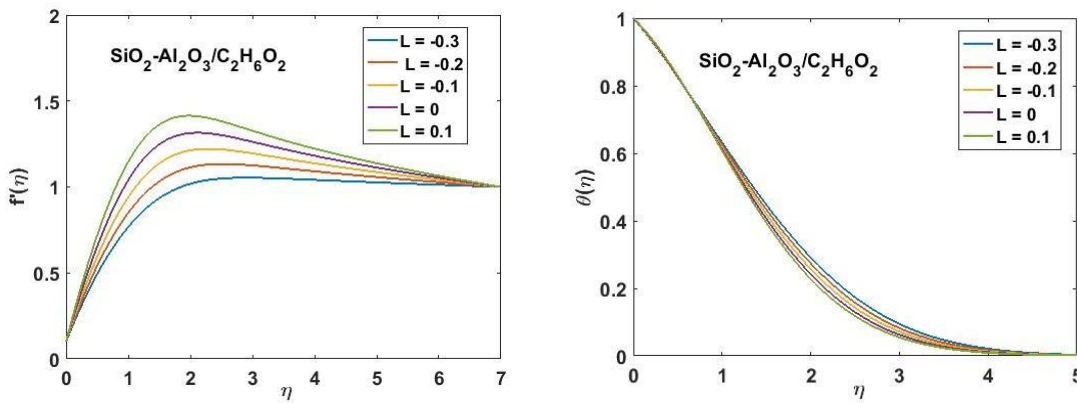
(a) Velocity profile $f'(\eta)$ for diverging amounts of L

(b) Thermal profile $\theta(\eta)$ for diverging amounts of L

Figure 5: Variation of λ on $f'(\eta)$ and $\theta(\eta)$.
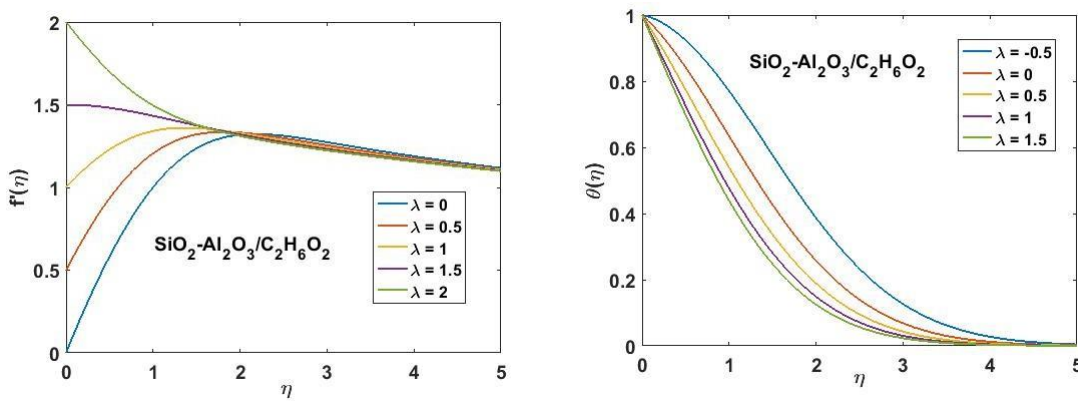
(a) The velocity profile $f'(\eta)$ for diverging amounts of λ

(b) Thermal profile $\theta(\eta)$ for diverging amounts of λ

Figure 6: Variation of φ_1 on $f(\eta)$ and $\theta(\eta)$.
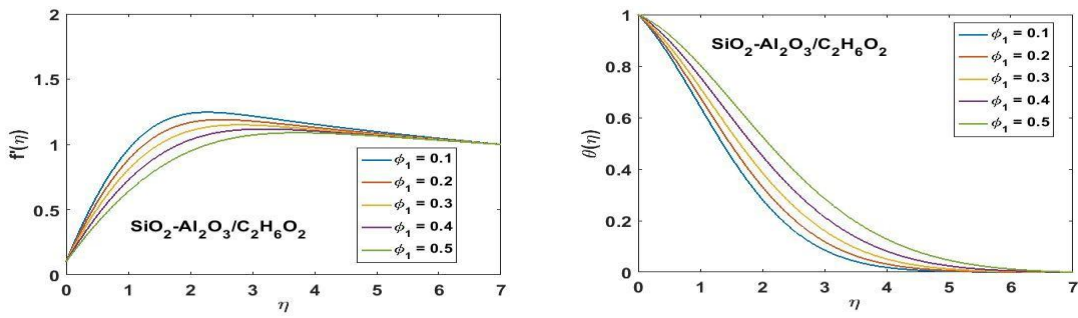
(a) Velocity profile $f(\eta)$ for diverging amounts of φ_1 (b) Thermal profile $\theta(\eta)$ for diverging amounts of φ_1

Figure 7: Variation of φ_2 on $f'(\eta)$ and $\theta(\eta)$.
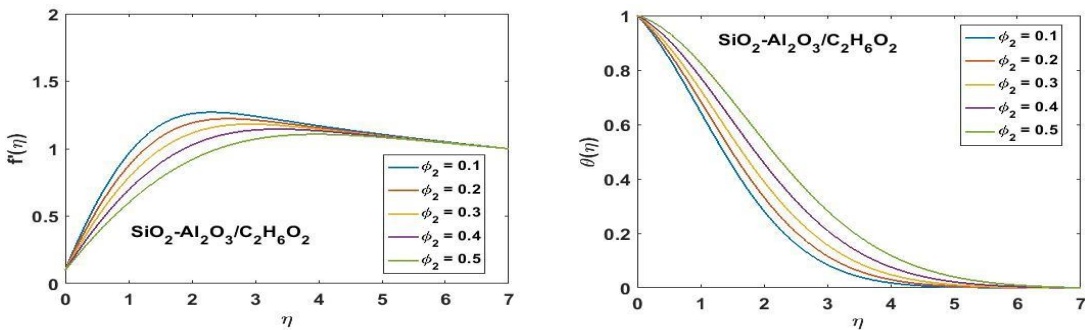
(a) Velocity profile $\theta(\eta)$ for diverging amounts of φ_2 (b) Thermal profile $\theta(\eta)$ for diverging amounts of φ_2

Figure 8: Variation of R, Ec and Pr on $\theta(\eta)$.
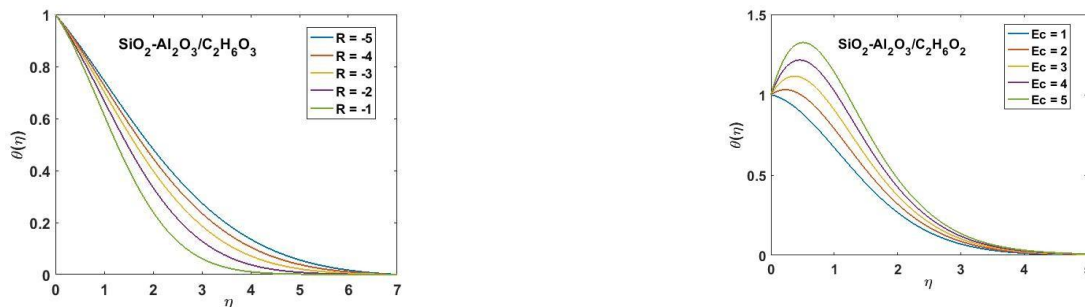
(a) Thermal profile $\theta(\eta)$ for diverging amounts of R (b) Thermal profile $\theta(\eta)$ for diverging amounts of Ec
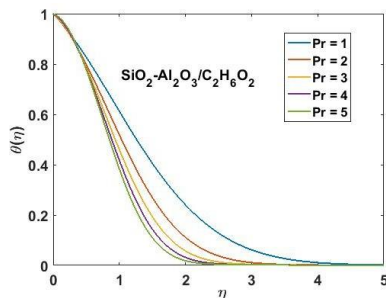
(c) Thermal profile $\theta(\eta)$ for diverging amounts of Pr

3   Concluding Remarks

A few of the study's most significant findings are as follows:

· The velocity distribution grows for larger values of m, Fr, L and λ and declines for stronger hybrid nanoparticles.

· The temperature field thickness is higher for λ, φ_1, φ_2 and Ec while decreases for higher values of m, Fr, L, R and Pr.

· The skin friction coefficient rises with rising amounts of φ_1, φ_2 and m.

· The local Nusselt number shows increasing behavior for increasing amounts of φ_1, φ_2,

Ethical Standards Compliance

Declaration of Originally

Since no one else has produced anything like this before, the author claims sole ownership of the data and graphics included in this report.

Conflict of Interest

There is no conflict of interest.

References

[1]   Falkner V. M., Skan S. W., (1931). Some appropriate solutions of the boundary layer equations. Phil. Mag., 12, 865-896.

https://doi.org/10.1080/14786443109461870

[2]   Hartree D. R., (1937). On an equation occurring in Falkner and Skan's approximate treatment of the equations of the boundary layer. Math. Proc. Camb. Phil. Soc., 2, 33, 223-239.

[3]   Stewartson K., (1954). Further solutions of the Falkner-Skan equation. Math. Proc. Camb. Phil. Soc., 50, 454-465.

[4]   Chen K. K., Libby P. A., (1968). Boundary layers with small departure from the Falkner-Skan profile. J. Fluid Mech., 33, 273-282.

[5]   Rajagopal K. R., Gupta A. S., Na T. Y., (1983). A note on the Falkner-Skan flows of a non-Newtonian fluid. I. J. Non-Linear Mech., 18, 313-320.

[6]   Botta E. F. F., Hut F. J., Veldman A. E. P., (1986). The role of periodic solutions in the Falkner-Skan problem for $\lambda > 0$. J. Eng. Math., 20, 81-93.

[7]   Brodie P., Banks W. H. H., (1987). Further properties of the Falkner-Skan equation. Acta Mech., 65, 205-211.

[8]   Heeg R. S., Dijkstra D., Zandbergen P. J., (1999). The stability of Falkner-Skan flows with several inflection points. J. Appl. Math. and Phys., 50, 82-93.

[9]   Zaturska M. B., Banks W. H. H., (2001). A new solution branch of the Falkner-Skan equation. Acta Mech., 152, 197-201.

[10]   Kumari M., Takhar H., S., Nath G., (2001). Mixed convection flow over a vertical wedge embedded in a highly porous medium. Heat Mass Transf., 37, 139-146.

[11]   Kuo B. L., (2003). Application of the differential transformation method to the solutions of Falkner-Skan wedge flow. Acta Mech., 164, 161-174.

[12]   Pantokratoras A., (2006). The Falkner-Skan flow with constant wall temperature and variable viscosity. I. J. Therm. Sci., 45, 378-389.

[13]   Ishak A., Nazar R., Pop I., (2006). Moving wedge and flat plate in a micro-polar fluid. Int. J. Eng. Sci., 44, 1225-1236.

[14] Vajravelu K., Nayfeh J., (1992). Hydromagnetic convection at a cone and a wedge. Int.Commun. Heat Mass Transf., 19, 701-710. http://dx.doi.org/10.1016/0735-1933(92)90052-j

[15] Chamkha A. J., Mujtaba M., Quadri A., Issa Camille, (2003). Thermal radiation effects on MHD forced convection flow adjacent to a non-isothermal wedge in the presence of aheat source or sink. Heat Mass Transf., 39, 305-312. http://dx.doi.org/10.1007/s00231-002-0353-4.

[16] Ahmad R., Khan W.A., (2013). Effect of viscous dissipation and internal heat generation/absorption on heat transfer flow over a moving wedge with convectiveboundary condition. Heat Transfer-Asian Res., 42, 589-602.10.1002/htj.21055

[17] Ibrahim W., Tulu A., (2019). Magnetohydrodynamic (MHD) boundary layer flow past a wedge with heat transfer and viscous effects of nanofluid embedded in porous media. Mathemat. Probl. Eng., 2019, 1-12. 10.1155/2019/4507852.

[18] Bano N., Singh B. B., Sayyed, S. R., (2020). MHD Heat Transfer Flow of Casson Fluid with Velocity and Thermal Slips over a Stretching Wedge in the Presence of Thermal Radiation. Diff. Found., 26, 1-22.10.4028/www.scientific.net/DF.26.1.

[19] Minea A. A., (2016). A review on the thermophysical properties of water-based nanofluids and their hybrids. Te Annals of "DUNAREA DE JOS" University of GALATI, 083X, 35-47.

[20] Sarkar J., Ghosh P.,Adil A., (2015). A review on hybrid nanofluids: recent research, development and applications. Ren. and Sust. Energy Reviews, 43,164-177.

[21] Sunder L. S., Sharma K. V., Singh M. K., Sousa A. C. M., (2017). Hybrid nanofluids preparation, thermal properties, heat transfer and friction factor- a review. Ren. and Sust.Energy Reviews, 68, 185-198.

[22] Sidik N. A. C., Adamu I. M.,Jamil M. M., Kefayati G. H. R., Mamat R., Najafi G., (2016).Recent progress on hybrid nanofluids in heat transfer applications: a comprehensive Review. International Communications in Heat Mass Transf., 78, 68-79.

[23] Sajid M. U., Ali H. M., (2018). Thermal conductivity of hybrid nanofluids: a critical review. International journal of Heat Mass Transf., 126, 211-234.

[24] Devi S. P. A., Devi S. S. U., (2016). Numerical investigation of hydromagnetic hybrid $Cu - Al_2O_3$/water nanofluid flow over a permeable stretching sheet with suction. I. J. ofNonlinear Sci. and Num. Simul., 17, 249-257.

[25] Devi S. P. A., Devi S. S. U., (2016). Numerical investigation of three-dimensional hybrid$Cu-Al_2O_3$/water nanofluid flow over a stretching sheet with effecting Lorentz force subjectto Newtonian heating. Canad. J. Phys., 94, 490-496.

[26] Adriana M. A., (2017). Hybrid nanofluids based on Al_2O_3, TiO_2, and SiO_2: numerical evaluation of different approaches. I. J. of Heat Mass Transf., 104, 852-860.

[27] Rostami M. N., Dinarvand S., Pop I., (2018). Dual solution for mixed convectivestagnation-point flow of an aqueous silica-alumina hybrid nanofluid. Chin. J. Phys., 56, 2465-2478.

[28] Ghadikolaei S. S., Gholinia M., Hoseini M. E., Ganji D. D., (2019). Natural convective MHD flow due to MoS_2-Ag nanoparticles suspended in $C_2H_6O_2-H_2O$ hybrid base fluid with thermal radiation. J. Taiwan Inst. Chem. Eng. 97, 12-23.

[29] Mackolil J., Mahanthesh B., (2019). Time-dependent nonlinear convective flow and radiative heat transfer of $Cu-Al_2O_3-H_2O$ hybrid nanofluidwith polar particles suspension:astatistical and exact analysis. Bio Nano Sci., 9, 937-951.

[30] Ashlin T. S., Mahanthesh B., (2019). Exact solution of non-coaxial rotating and non-linear convective flow of $Cu-Al_2O_3-H_2O$ hybrid nanofluids over an infinite vertical plate subjected to heat source and radiative heat. J. nanofluids, 8, 781-794.

[31] Imtiaz M., Shahid F., Hayat T., Alsaedi A., (2019). Melting heat transfer in Cu-water andAg-water nanofuids flow. Appl. Math. Mech. (English Edition), 40, 465-480. https://doi.org/10.1007/s10483-019-

2462-8

[32] Mohebbi R. IzadiM. Delouei A. A., Sajjadi H., (2019). Effect of MWCNT-Fe_3O_4/water hybrid nanofluido on the thermal performance of ribbed channel with apart sections of heating and cooling. J. Therm. Anal. Calorim., 135, 3029-3042.

[33] Tiwari R. K., Das M. K., (2007). Heat transfer augmentation in a two-sided lid-driven differentially heated square cavity utilizing nanofluids. Int. J. Heat Mass Transf., 50, 2002–2018.

10.1016/j.ijheatmasstransfer.2006.09.034

[34] Syam Sundar L., Sharma K. V., Singh M. K., Sousa, A. C. M., (2017). Hybrid nanofuids preparation, thermal properties, heat transfer and friction factor – A review. Renew. Sustain. Energy Rev. 68, 185-198.

[35] Ghadikolaei S. S., Yassari M., Sadeghi H., Hosseinzadeh K., Ganji, D. D., (2017). Investigation on thermophysical properties of $TiO_2–Cu/H_2O$ hybrid nanofluid transport dependent on shape factor in MHD stagnation point flow. Powder Tech., 322, 428-438.

[36] Hayat T., Nadeem S. (2017). Heat transfer enhancement with Ag-CuO/water hybrid nanofuid. Results Phys., 7, 2317-2324.

[37] Mjankwi M. A., Masanja V. G., Mureithi E. W., James M. N., (2019). Unsteady MHD flow of nanofluid with variable properties over a stretching sheet in the presence of thermal radiation and chemical reaction. Int. J. Math. and Math. Sci., 2019.

[38] Khan U., Zaib A., Oudina F. M., (2020). Mixed convective magneto flow of $SiO_2 -MoS_2/C_2H_6O_2$ hybrid nano liquids through a vertical stretching/shrinking wedge: stability analysis. Arab. J. Sci. and Eng., 45, 9061-9063.10.1007/s13369-020-04680-7

[39] Waini I., Ishak A., Pop I., (2019). MHD flow and heat transfer of a hybrid nanofluid pasta permeable stretching/shrinking wedge. Applied Math. and Mech.10.1007/s10483-020-2584-7

[40] White F. M., (1991). Viscous Fluid Flow, McGraw-Hill, New York, NY, USA, 2nd edition.

[41] Khan W. A., Pop I., (2013). Boundary Layer Flow Past a Wedge Moving in a Nanofluid.Math. Prob. Eng., 2013. 10.1155/2013/637285

[42] Blasius H., (1908). "Grenzschichten in Flussigkeiten mit kleiner Reibung," ZentralblattMathematical Physics, 56, 1–37.